Achieving Uniform Mixing in a Microfluidic Device: Hydrodynamic Focusing Prior to Mixing

Hye Yoon Park, Xiangyun Qiu, Elizabeth Rhoades, Jonas Korlach, Lisa W. Kwok, Warren R. Zipfel, Watt W. Webb, and Lois Pollack*

School of Applied and Engineering Physics, Cornell University, Ithaca, New York 14853

We describe a microfluidic mixer that is well-suited for kinetic studies of macromolecular conformational change under a broad range of experimental conditions. The mixer exploits hydrodynamic focusing to create a thin jet containing the macromolecules of interest. Kinetic reactions are triggered by molecular diffusion into the jet from adjacent flow layers. The ultimate time resolution of these devices can be restricted by premature contact between co-flowing solutions during the focusing process. Here, we describe the design and characterization of a mixer in which hydrodynamic focusing is decoupled from the diffusion of reactants, so that the focusing region is free from undesirable contact between the reactants. Uniform mixing on the microsecond time scale is demonstrated using a device fabricated by imprinting optical-grade plastic. Device characterization is carried out using fluorescence correlation spectroscopy (FCS) and two-photon microscopy to measure flow speeds and to quantify diffusive mixing by monitoring the collisional fluorescence quenching, respectively. Criteria for achieving microsecond time resolution are described and modeled.

Kinetic studies of rapid conformational changes provide valuable insights into the mechanisms of macromolecular self-assembly (e.g., protein or RNA folding). A thorough understanding of the folding pathways requires investigation of the earliest folding steps that form the foundation for all subsequent events. Remarkable innovations have therefore evolved for probing folding on rapid time scales, relying on techniques such as photochemical triggering, temperature/pressure jump, or rapid fluid mixing methods (reviewed in refs 1 and 2). In the latter technology, which is the subject of this paper, folding transitions are triggered by an abrupt change of the solvent around the macromolecules.

Fluid mixers are compatible with a wide range of experimental conditions and have been coupled with numerous detection methods;[2] however, commercially available devices have limited time resolution, of order 1 ms. Because interesting kinetics often occurs on shorter time scales, innovative mixer designs have been introduced to access this regime. For example, turbulence has been used to facilitate rapid mixing in either continuous-flow[3−9] or quenched-flow[10,11] devices by creating eddies that reduce the length scale for diffusion. However, the high flow rates required to induce turbulence are undesirable when limited amounts of the biological sample are available.

At the lower flow rates that conserve sample, rapid mixing without turbulence is possible when the length scale for diffusion is reduced by hydrodynamic focusing.[12] Knight et al.[13] demonstrated a laminar flow mixer, in which a solution containing macromolecules is confined into a thin "jet" by a second solution flowing from two orthogonal channels. Low molecular weight reactants in the second solution rapidly diffuse into the thin jet and trigger folding of the macromolecules. This mixer has been successfully used in protein and RNA folding studies in conjunction with small-angle X-ray scattering (SAXS),[14−16] Fourier transform IR (FTIR) spectroscopy,[17] UV fluorescence spectroscopy,[18] and Förster resonance energy transfer (FRET).[19−21] The method

* Corresponding author. E-mail: lp26@cornell.edu. Phone: 607-255-8695. Fax: 607-255-7658.

(1) Eaton, W. A.; Munoz, V.; Hagen, S. J.; Jas, G. S.; Lapidus, L. J.; Henry, E. R.; Hofrichter, J. *Annu. Rev. Biophys. Biomol. Struct.* **2000**, *29*, 327−359.
(2) Roder, H.; Shastry, M. C. R. *Curr. Opin. Struct. Biol.* **1999**, *9*, 620−626.
(3) Regenfuss, P.; Clegg, R. M.; Fulwyler, M. J.; Barrantes, F. J.; Jovin, T. M. *Rev. Sci. Instrum.* **1985**, *56*, 283−290.
(4) Takahashi, S.; Yeh, S. R.; Das, T. K.; Chan, C. K.; Gottfried, D. S.; Rousseau, D. L. *Nat. Struct. Biol.* **1997**, *4*, 44−50.
(5) Chan, C. K.; Hu, Y.; Takahashi, S.; Rousseau, D. L.; Eaton, W. A.; Hofrichter, J. *Proc. Natl. Acad. Sci. U.S.A.* **1997**, *94*, 1779−1784.
(6) Shastry, M. C. R.; Luck, S. D.; Roder, H. *Biophys. J.* **1998**, *74*, 2714−2721.
(7) Grigoryants, V. M.; Veselov, A. V.; Scholes, C. P. *Biophys. J.* **2000**, *78*, 2702−2708.
(8) Akiyama, S.; Takahashi, S.; Kimura, T.; Ishimori, K.; Morishima, I.; Nishikawa, Y.; Fujisawa, T. *Proc. Natl. Acad. Sci. U.S.A.* **2002**, *99*, 1329−1334.
(9) Bilsel, O.; Kayatekin, C.; Wallace, L. A.; Matthews, C. R. *Rev. Sci. Instrum.* **2005**, *76*, 014302.
(10) Bökenkamp, D.; Desai, A.; Yang, X.; Tai, Y. C.; Marzluff, E. M.; Mayo, S. L. *Anal. Chem.* **1998**, *70*, 232−236.
(11) Lin, Y.; Gerfen, G. J.; Rousseau, D. L.; Yeh, S. R. *Anal. Chem.* **2003**, *75*, 5381−5386.
(12) Brody, J. P.; Yager, P.; Goldstein, R. E.; Austin, R. H. *Biophys. J.* **1996**, *71*, 3430−3441.
(13) Knight, J. B.; Vishwanath, A.; Brody, J. P.; Austin, R. H. *Phys. Rev. Lett.* **1998**, *80*, 3863−3866.
(14) Pollack, L.; Tate, M. W.; Darnton, N. C.; Knight, J. B.; Gruner, S. M.; Eaton, W. A.; Austin, R. H. *Proc. Natl. Acad. Sci. U.S.A.* **1999**, *96*, 10115−10117.
(15) Pollack, L.; Tate, M. W.; Finnefrock, A. C.; Kalidas, C.; Trotter, S.; Darnton, N. C.; Lurio, L.; Austin, R. H.; Batt, C. A.; Gruner, S. M.; Mochrie, S. G. J. *Phys. Rev. Lett.* **2001**, *86*, 4962−4965.
(16) Russell, R.; Millettt, I. S.; Tate, M. W.; Kwok, L. W.; Nakatani, B.; Gruner, S. M.; Mochrie, S. G. J.; Pande, V.; Doniach, S.; Herschlag, D.; Pollack, L. *Proc. Natl. Acad. Sci. U.S.A.* **2002**, *99*, 4266−4271.
(17) Kauffmann, E.; Darnton, N. C.; Austin, R. H.; Batt, C.; Gerwert, K. *Proc. Natl. Acad. Sci.U.S.A.* **2001**, *98*, 6646−6649.
(18) Pabit, S. A.; Hagen, S. J. *Biophys. J.* **2002**, *83*, 2872−2878.
(19) Lipman, E. A.; Schuler, B.; Bakajin, O.; Eaton, W. A. *Science* **2003**, *301*, 1233−1235.
(20) Dittrich, P. S.; Müller, B.; Schwille, P. *Phys. Chem. Chem. Phys.* **2004**, *6*, 4416−4420.

10.1021/ac060572n CCC: $33.50
Published on Web 05/17/2006

of hydrodynamic focusing has been also adapted in other microfluidic devices to suppress nonspecific adsorption of the sample,[22] confine the sample delivery,[23,24] or enhance mixing in lab-on-a-chip applications.[25]

Previous hydrodynamic focusing mixers[13,21] concentrated on achieving the shortest mixing time by reducing the width of the jet to minimize the length scale for diffusion. However, as discussed here, accurate determination of the time resolution of the mixer also requires careful examination of systematic errors, which have been mostly overlooked in previous studies. In particular, premature mixing prior to formation of the focused jet, referred to as "premixing",[13] causes a large variation in the mixing progress. This effect becomes more pronounced for microsecond-range measurements. This detrimental problem can be reduced to some extent by the use of smaller channels or a nozzle.[13,21] However these approaches are constrained by the minimum feature size of fabrication methods (~1 μm in the case of photolithography). In addition, troublesome clogging issues arise in small channels. An alternative approach relies on flowing the solution more rapidly through the focusing region. However, sample consumption increases with flow rate. Furthermore the shear force resulting from fast flow through a small channel may affect the structure of the biomolecules, complicating the folding event.[4,6,9]

Here we demonstrate a new five-inlet port mixer that addresses the premixing issues present in previous hydrodynamic focusing mixers. Sheath flow is used to create a barrier between the two reactants during the focusing process. We show that small amounts of sheath flow effectively reduce premixing without compromising rapid mixing by diffusion. The fabrication of an optically transparent plastic mixer by imprinting is described, as well as its characterization with fluorescence correlation spectroscopy (FCS) and collisional quenching of fluorescent dye.

EXPERIMENTAL SECTION

Device Fabrication. A schematic of the five-inlet port mixer is shown in Figure 1. Macromolecules in their initial state in solution A are injected into the center channel. Solution B flows into two side channels, and solution A (without macromolecules) flows in the diagonal channels. The angle between the center and the diagonal channels is 45°. The overall dimensions of the plastic mixer are 1.5 cm × 1.5 cm × 0.1 cm, and the channels are 50 μm wide and 100 μm deep. The 1:2 (width:depth) aspect ratio of the channel maintains a relatively uniform flow speed of the sample through the two-photon focal volume, which has a lateral radius of 250 nm and an axial radius of 1.5 μm with 780 nm excitation wavelength.[26] In this geometry, complications that arise from the parabolic flow profile in the *z*-direction are minimized.

The microstructures were imprinted on Zeonor 1020R (Zeon Chemicals L. P., Louisville, KY) following a method described by

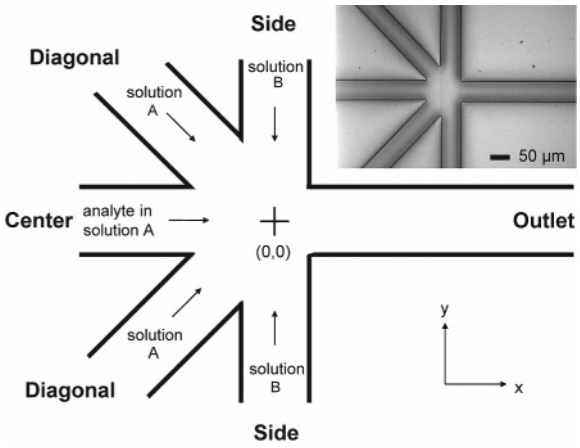

Figure 1. Schematic of the mixer (top down view). The origin is set at the crossing point of the side channels and the center channel. The inset shows a light microscopy image of the plastic microfluidic mixer. Each channel is 50 μm wide and 100 μm deep.

Kameoka et al.[27] A raised pattern was fabricated on a silicon wafer using contact photolithography and deep reactive ion etching. A 2 mm thick Zeonor 1020R plaque was cut into the appropriate size and cleaned with acetone. The polymer chip was placed on the silicon mold and pressed with 150 psi at 130 °C for 10 min. The imprinted chip was sealed with a glass coverslip coated with a thin layer of RTV 615 (GE silicones, Waterford, NY).

Sample Delivery. The microfluidic mixer was interfaced to external syringe pumps (PHD 2000, Harvard Apparatus, Holliston, MA) through a custom-built holder. The holder accepts standard PTFE tubing and, through a series of internally machined channels, directs the flow into the channels of the mixer. O-rings were inserted between the microfluidic chip and the holder, and a cover plate was attached with screws, providing compression to make the system leak tight. This assembly was mounted on a microscope stage for fluorescence imaging and FCS measurements.

Premixing Detection with Ca-Sensitive Dye. Prevention of premixing by diagonal sheath flow was demonstrated using a Ca-sensitive dye to report Ca^{2+} ion concentration. Samples of 10 μM Ca-Green 5N, 5 μM Cascade Blue dextran conjugate 70 kDa, and 10 mM $CaCl_2$ were injected into the center channel, diagonal channels, and side channels, respectively. All solutions were prepared in 25 mM Mops at pH 7, 150 mM KCl, 0.1 mg/mL BSA, and 0.1 mM EGTA.

Fluorescence images were obtained using multiphoton microscopy. The excitation wavelength was 800 nm and a 20×/0.75 NA water immersion objective lens (Olympus) was used in conjunction with a 670UVDCLP dichroic beam splitter, BGG22 emission filter, D525/50 band-pass filter (Chroma Technology Corp., Rockingham, VT), and GaAsP photomultiplier tubes (H7421, Hamamatsu, Bridgewater, NJ).

Flow Speed Measurements with Fluorescence Correlation Spectroscopy (FCS). Flow speed profiles inside the mixer were measured with FCS. FCS measures the fluctuations in the number of fluorescent molecules in a small focal volume of ~3 μm^3. With the high spatial resolution of FCS, three-dimensional flow profiles in a microfluidic channel can be measured precisely.[28–33]

(21) Hertzog, D. E.; Michalet, X.; Jäger, M.; Kong, X.; Santiago, J. G.; Weiss, S.; Bakajin, O. *Anal. Chem.* **2004**, *76*, 7169–7178.
(22) Munson, M. S.; Hasenbank, M. S.; Fu, E.; Yager, P. *Lab Chip* **2004**, *4*, 438–445.
(23) Hofmann, O.; Voirin, G.; Niedermann, P.; Manz, A. *Anal. Chem.* **2002**, *74*, 5243–5250.
(24) Sundararajan, N.; Pio, M. S.; Lee, L. P.; Berlin, A. A. *J. Microelectromech. Syst.* **2004**, *13*, 559–567.
(25) Nguyen, N. T.; Huang, X. *Lab Chip* **2005**, *5*, 1320–1326.
(26) Zipfel, W. R.; Williams, R. M.; Webb, W. W. *Nat. Biotechnol.* **2003**, *21*, 1369–1377.
(27) Kameoka, J.; Craighead, H. G.; Zhang, H.; Henion, J. *Anal. Chem.* **2001**, *73*, 1935–1941.

A sample of 10 nM Rhodamine Green (Molecular Probes, Eugene, OR) in HPLC water was injected into the five inlet ports of the mixer. The mixer was mounted onto an inverted microscope (IX71, Olympus, Melville, NY) equipped with an MS2000 microscope stage (Applied Scientific Instrumentation, Eugene, OR). A 488 nm solid-state diode-pumped laser (Sapphire 488−20, Coherent Inc., Santa Clara, CA) excited the dye molecules. The beam was focused onto the channel by a 40×/1.15 NA water immersion objective lens (Olympus). The laser power at the sample was 30 and 140 μW, for diffusion and flow measurements, respectively. The fluorescence passed through a dichroic beam splitter and a long-pass filter (510DCLP and 510LP, Chroma Technology Corp., Rockingham, VT) and was imaged onto a 50 μm core, 50/50 fiber splitter (Oz Optics, Carp, ON, Canada). The two output ends of the fiber were coupled to two identical avalanche photodiodes (PerkinElmer Optoelectronics, Fremont, CA). The signals from two outputs were cross-correlated by a correlator card (Correlator.com, Bridgewater, NJ) in order to eliminate the artifacts from detector afterpulsing at short time scales. The data acquisition time at each location within the mixer was 10 s, and three to five curves were averaged.

We determined the $1/e^2$ focal radius of the beam, r_0, using the diffusion coefficient of Rhodamine Green, $D_{RG} = (3.01 \pm 0.08) \times 10^{-6}$ cm^2/s,[34] in the absence of the driven flow. For the flow speed measurement, FCS curves were fit using a model of uniform translation with diffusion:

$$G_{\text{diff\&flow}}(\tau) = \frac{1}{N}\left(1 + \frac{\tau}{\tau_{\text{diff}}}\right)^{-1}\left(1 + \frac{\tau}{w^2\tau_{\text{diff}}}\right)^{-1/2} \times \exp\left\{-\left(\frac{\tau}{\tau_{\text{flow}}}\right)^2\left(1 + \frac{\tau}{\tau_{\text{diff}}}\right)^{-1}\left(1 + \frac{\tau}{w^2\tau_{\text{diff}}}\right)^{-1/2}\right\} \quad (1)$$

where N is the average number of molecules in the focal volume, τ_{diff} is the characteristic diffusion time, w is the ratio of axial to lateral dimensions of the focal volume, and τ_{flow} is the characteristic flow time.[28,29] τ_{diff} and w were fixed at the values obtained from the measurement in the absence of the flow. N and τ_{flow} were obtained from the best fit to each FCS curve. Finally, the flow speed V was calculated from $V = r_0/\tau_{\text{flow}}$.

Concentration Measurements with Collisional Quenching of Fluorescence. Diffusive mixing in the device was quantified by measuring the collisional quenching of fluorescent dye with potassium iodide (KI),[13] a diffusion-limited process. As iodide ions from the side channels diffuse into the jet, they collide with fluorophores and quench fluorescence. The effect is governed by the Stern−Volmer equation:

$$\frac{F_0}{F} = 1 + k_{\text{SV}}[\text{KI}] \quad (2)$$

where F and F_0 are the fluorescence intensities with and without quenching, respectively, and k_{SV} is the Stern−Volmer quenching constant.[35] A sample of 50 μM Alexa fluor 488 dextran conjugate 10 kDa (Molecular Probes, Eugene, OR) was used as a fluorophore; the dextran conjugated dye with the increased molecular weight mimics the slower diffusion of macromolecules; 125 mM potassium iodide was used as a quencher. All solutions were prepared in 1.25 mM sodium thiosulfate and 50 mM Tris-HCl buffer at pH 8.5. Sodium thiosulfate was added to prevent formation of iodine.

Fluorescence images were obtained using multiphoton microscopy. The multiphoton microscope setup was based on an inverted microscope (IX70, Olympus, Melville, NY) and a Bio-Rad MRC-1024 scan box (Hempstead, U. K.). A ~100 fs pulsed Ti:Sapphire laser, mode-locked at 780 nm was guided into the microscope. The average power at the sample was ~30 mW. A 20×/0.7 NA water immersion objective (Olympus) was used with a 670UVDCLP dichroic beam splitter and D525/50 band-pass filter (Chroma Technology Corp., Rockingham, VT). The signal was collected by bi-alkali photomultiplier tubes (HC 125-02, Hamamatsu). For each flow speed condition, 10 images were scanned and averaged.

To calibrate the Stern−Volmer quenching constant, fluorescence of the dye at different KI concentrations (0, 20, 40, 60, 80, 100, and 120 mM) and the background in the absence of fluorophore were measured using Lab-Tek chambered coverglass (Nalge Nunc International, Rochester, NY) on the multiphoton microscope setup. After the calibration, the microfluidic mixer complex was mounted on the microscope and the fluorescence change of the dye due to diffusive mixing with quencher was monitored. Dextran conjugated Alexa 488 in Tris buffer was injected into the center channel, and Tris buffer was injected into the diagonal channels as sheath flow. Into the side channels, Tris buffer was introduced first to collect unquenched data. Then 125 mM KI solution was infused into the side channels to quench the fluorescence. The fluorescence intensity along the jet was background subtracted, normalized to the intensity in the upstream of the center channel before mixing, and averaged over 5−20 μm in x-direction. More averaging was employed for thinner jets to suppress the noise. The local concentration of KI along the focused jet was calculated using eq 2.

THEORETICAL MODEL

To assess the benefits of the new design (Figure 1), numerical simulations were employed to quantify the mixing performance of a hydrodynamic focusing mixer in both the presence and absence of the sheath flow. Within these mixers, the flow velocity $\vec{V}$ is governed by the steady-state incompressible Navier−Stokes equation:

$$\rho(\vec{V}\cdot\nabla)\vec{V} = -\nabla P + \eta\nabla^2\vec{V} \quad (3)$$

where ρ is the fluid density, P is the pressure, and η is the dynamic

(28) Magde, D.; Webb, W. W.; Elson, E. L. *Biopolymers* **1978**, *17*, 361−376.
(29) Gösch, M.; Blom, H.; Holm, J.; Heino, T.; Rigler, R. *Anal. Chem.* **2000**, *72*, 3260−3265.
(30) Dittrich, P. S.; Schwille, P. *Anal. Chem.* **2002**, *74*, 4472−4479.
(31) Foquet, M.; Korlach, J.; Zipfel, W.; Webb, W. W.; Craighead, H. G. *Anal. Chem.* **2002**, *74*, 1415−1422.
(32) Lenne, P. F.; Colombo, D.; Giovannini, H.; Rigneault, H. *Single Mol.* **2002**, *3*, 194−200.
(33) Kuricheti, K. K.; Buschmann, V.; Weston, K. D. *Appl. Spectrosc.* **2004**, *58*, 1180−1186.
(34) Hess, S. T.; Webb, W. W. *Biophys. J.* **2002**, *83*, 2300−2317.
(35) Lakowicz, J. R. *Principles of Fluorescence Spectroscopy*, 2nd ed.; Kluwer Academic/Plenum Publishers: New York, 1999.

viscosity.[36] The local concentration of the reactant is obtained from the diffusion and convection equation:

$$\vec{V}\cdot\nabla C = D\nabla^2 C \tag{4}$$

where D is the diffusion coefficient of the reactant, and C is the reactant concentration.[36] The two partial differential equations with boundary conditions appropriate for each mixer are numerically solved with a finite element method, using the commercial program Comsol Multiphysics (Comsol Inc., Stockholm, Sweden). Simulations were carried out using the diffusion coefficient of iodide ions, $D = 2.045 \times 10^{-5}$ cm^2/s,[37] for direct comparison with the experimental data measuring collisional quenching of fluorescent dye by iodide.

To quantify the mixer performance, we traced approximately 1000 streamlines in the vertical mid-plane originating from the center channel. Since the typical width of the focused jet (50 nm to 1 μm) is smaller than or comparable to the detection beam size, any single measurement samples all molecules across the width of the jet. We assume that the streamlines represent the trajectory of the macromolecules because the flow is laminar (Reynold's number is lower than 30) and the transverse diffusion of the large macromolecules is negligible on the time scale of our experiments. At each location (each value of x in Figure 1), the distribution of elapsed time is calculated by summing the contribution of all streamlines; for the ith streamline at location x, we calculate the elapsed time $t_i(x)$ of the streamline as follows. We assume that the reaction is triggered at a threshold concentration C_0. $t_i(x)$ is set to zero before the position $x0_i$ where $C = C_0$; at subsequent positions, the elapsed time t_i(x) equals the travel time from $x0_i$ to x. It is important to note that each streamline reaches this threshold at a different position $x0_i$. The distribution of time elapsed since each individual streamline crosses the threshold concentration yields two useful quantities at each position x, the average time:

$$\langle t(x)\rangle = \frac{\sum_i t_i(x)\, w_i(x)}{\sum_i w_i(x)} \tag{5}$$

and the standard deviation:

$$\sigma_t(x) = \sqrt{\frac{\sum_i (t_i(x) - \langle t(x)\rangle)^2 w_i(x)}{\sum_i w_i(x)}} \tag{6}$$

where $w_i(x)$ is the width of the ith streamline. We use the average time $\langle t(x)\rangle$ to convert the x coordinate into the time coordinate. The standard deviation of the elapsed time $\sigma_t(x)$ is regarded as the figure of merit for the mixing uniformity.

(36) Landau, L. D.; Lifshitz, E. M. *Fluid Mechanics*; Pergamon Press: London, 1959.

(37) Lide, D. R. *CRC Handbook Chemistry and Physics*, 85th ed.; CRC Press: Boca Raton, FL, 2004.

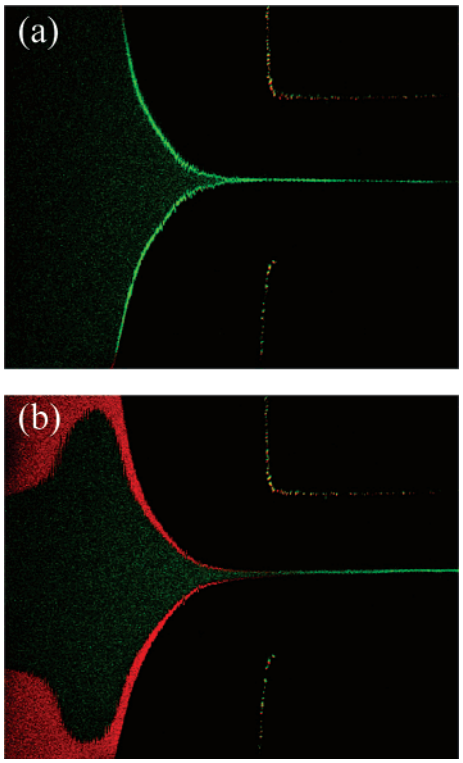

Figure 2. Prevention of premixing by diagonal sheath flow. (a) Without the sheath layer, mixing starts along the boundary of the central flow stream, before focusing is complete. The fluorescence intensity of Ca-sensitive dye at the boundary increases (bright green) due to Ca^{2+} binding. (b) With the sheath flow, Ca-sensitive dye remains distant from Ca^{2+} ions along the edges of the focusing region. Therefore protection by the sheath flow is achieved during hydrodynamic focusing.

RESULTS AND DISCUSSION

Benefits of Sheath Flow. Figure 2 illustrates the reduction of premixing by sheath flow. With negligible flow (0.2% of the total flow rate, Figure 2a) into the diagonal channels, the device mimics a four-port mixer. In this experiment, Ca-sensitive dye flows in the center channel, and $CaCl_2$ flows in the side channels. The increased fluorescence near the boundary of the focusing region signals the diffusion of Ca^{2+} ions into the central stream, demonstrating the onset of mixing prior to focusing. A significant uncertainty arises in the kinetic measurement from this undesired premature mixing. With a slightly increased flow rate into the diagonal channels (0.3% of total flow rate, Figure 2b), the sheath prevents contact between Ca^{2+} ions and the Ca-sensitive dye during focusing. Thus the sheath flow effectively reduces premixing.

To quantify the effect illustrated in Figure 2, we carried out simulations to model the flow in mixers with and without the diagonal channels under otherwise identical flow conditions. Figure 3, panels a and b, shows half of the focusing regions of two different mixers to illustrate the simulation results. The two-dimensional color maps depict the concentration of small molecules present in solution B; representative streamlines from the center channel are drawn in gray. The total diffusion length of 1.6 μm equals the jet width alone in Figure 3a, and the jet width plus two sheath widths in Figure 3b. This size is comparable to jet widths used in the previous RNA folding studies.[16] The average

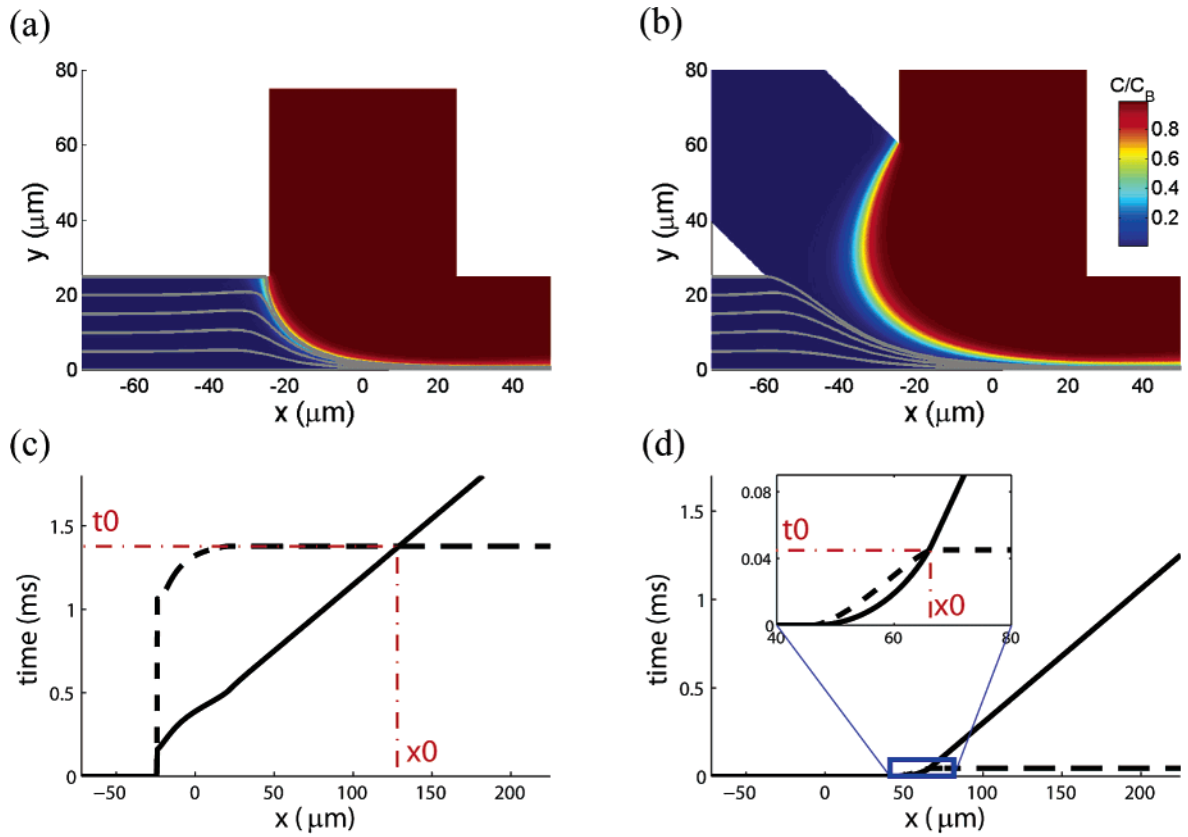

Figure 3. Two-dimensional simulation results of two different mixer designs (only one-half of each device is shown). The color plots depict the concentration of small molecules in the side channels as a fraction of the bulk concentration C_B. The streamlines from the center channel are in gray. (a) One-half of the mixer with two orthogonally crossed channels. The outer streamlines mix with side solution before a thin jet is formed. (b) One-half of the mixer with diagonal channels. (c and d) The average $\langle t(x) \rangle$ (solid line) and the standard deviation $\sigma_t(x)$ (broken line) of the elapsed time in the mixer of (a) and (b), respectively.

flow speed in the center channel is 4 mm/s, and the average flow speed in the side channel is 40 mm/s for both mixers. The average flow speed into the diagonal channel (Figure 3b) is 0.8 mm/s. The great variation in mixing in the absence of sheath flow is evident from Figure 3a; macromolecules flowing along the outer streamlines (toward the edge of the jet) contact reactant from the side channels long before those molecules flowing along inner streamlines (toward the center of jet). Thus a cross section of the jet contains a large variation in the local concentration of small molecules that have diffused from solution B. In strong contrast, Figure 3b shows that the sheath flow from the diagonal channel prevents mixing of macromolecules and solution B during focusing process.

The average elapsed time $\langle t(x) \rangle$ (solid line) and the standard deviation $\sigma_t(x)$ (dashed line) in each device are presented in Figure 3, panels c and d. The threshold concentration for mixing was set to 30%, an arbitrary choice but a reasonable value to model a published RNA folding study.[16] In the focusing region where the parabolic velocity profile broadens the distribution of elapsed time $t_i(x)$, both $\langle t(x) \rangle$ and $\sigma_t(x)$ increase as more streamlines gradually reach C_0; $\sigma_t(x)$ increases more rapidly than $\langle t(x) \rangle$ in this region because of the wide variation of flow speeds across the streamlines. Once the jet is fully focused and all streamlines reach the nearly constant final velocity, $\langle t(x) \rangle$ continues to increase linearly, but $\sigma_t(x)$ stays essentially constant. Consequently there exists a cross point $x0$, where $\langle t(x0) \rangle = \sigma_t(x0)$, shown in Figure 3, panels c and d. The time $t0 = \langle t(x0) \rangle$ marks the earliest point for a measurement with certainty. In the absence of sheath flow (Figure 3a), $x0 = 130$ μm and $t0 = 1.4$ ms, which is consistent with the time resolution of the previous RNA folding experiment with SAXS.[16] For data acquired at $x < 130$ μm, the error arising from nonuniform mixing exceeds the average elapsed time for macromolecules in the jet. This error is significantly reduced in the presence of sheath flow (Figure 3b). The crossing point shifts to $x0 = 66$ μm, which corresponds to the average elapsed time as early as 44 μs. These numbers obviously depend on both the flow rates as well as the diffusion coefficient of the low molecular weight species. Under these experimental conditions the presence of sheath flows improves the time resolution by a factor of 30.

Device Performance. The three most important parameters that determine device performance are sheath width, jet flow speed, and jet width. They can be easily controlled by changing the settings on the syringe pump to adjust the flow rates (volume per unit time) into the center (Q_c), diagonal (Q_d), and side channels (Q_s). In this section, we discuss the effect of varying these parameters.

(a) Sheath Width. The width of the sheath is established by the fraction of fluid that flows into the diagonal channels. The ratio Q_d/Q_{tot} is a critical parameter in determining the mixer operation; the sheath must be thick enough to prevent premixing, yet thin enough to allow reactant molecules to quickly diffuse through after focusing is complete. We used numerical simulations to identify an ideal condition for this balance. Simulation results are shown in Figure 4 as plots of mixing uniformity (Figure 4a)

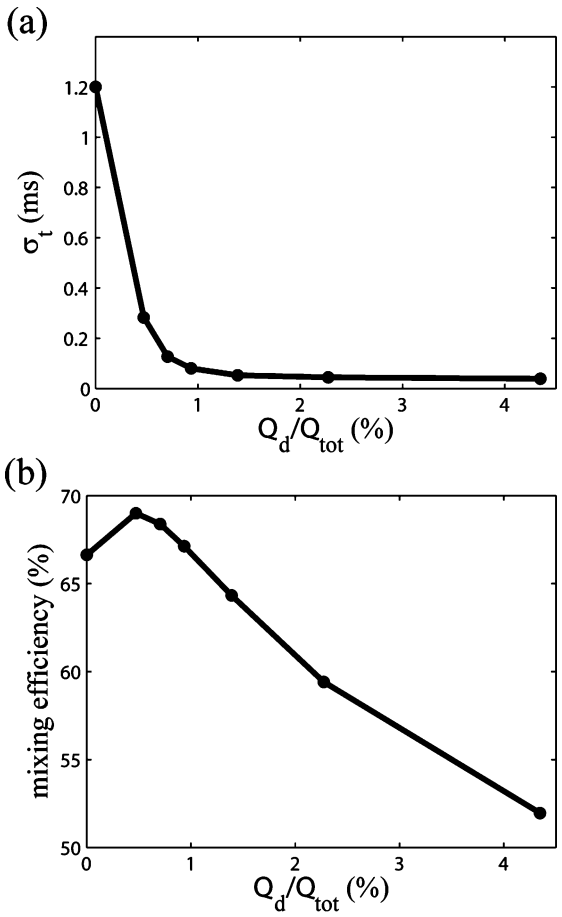

Figure 4. Mixing uniformity and mixing efficiency vs the ratio of Q_d to Q_{tot}. Simulations were performed for flow with $Q_c = 1$ μL/min and $Q_s = 10$ μL/min, while varying Q_d from 0 to 1 μL/min. The data for $Q_d = 0$ is from the mixer without diagonal channels. (a) The uncertainty in the elapsed time at $\langle t \rangle = 1$ ms as a function of Q_d/Q_{tot}. As the diagonal flow rate is increased, the uncertainty drops sharply at first and levels off around $Q_d/Q_{tot} = 1\%$. (b) Mixing efficiency at $\langle t \rangle = 1$ ms as a function of Q_d/Q_{tot}. The efficiency is higher with thinner sheath.

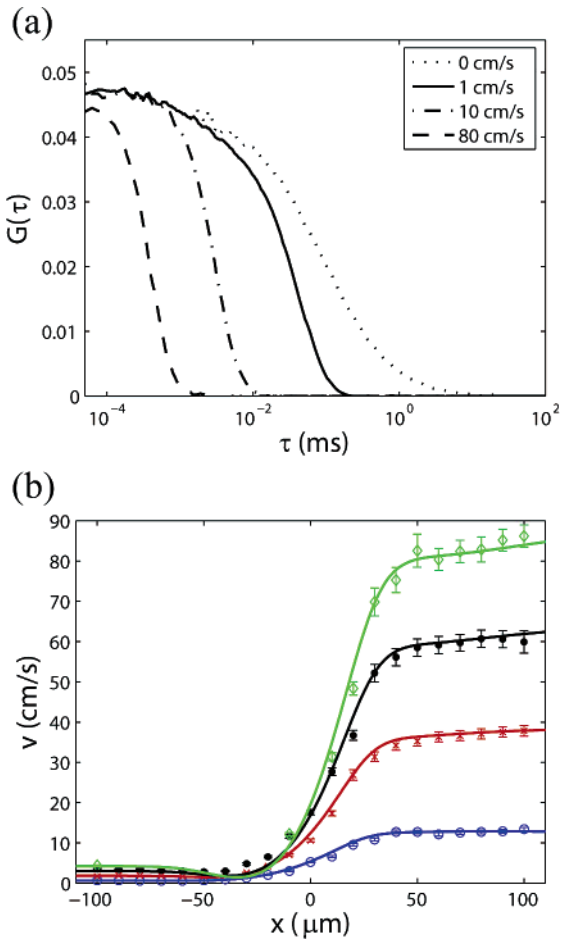

Figure 5. Flow speed measurements with FCS. (a) Cross-correlation curves at various flow speeds. The dotted curve corresponds to the condition where the syringe pumps are stopped. (b) Flow speed vs x at $y = 0$ and $z = 0$. Blue circles: $Q_c = 1$ μL/min, $Q_d = 0.2$ μL/min, and $Q_s = 10$ μL/min. Red crosses: $Q_c = 3$ μL/min, $Q_d = 0.5$ μL/min, and $Q_s = 30$ μL/min. Black dots: $Q_c = 5$ μL/min, $Q_d = 1.2$ μL/min, and $Q_s = 50$ μL/min. Green diamonds: $Q_c = 7$ μL/min, $Q_d = 1.5$ μL/min, and $Q_s = 70$ μL/min. Each solid line is the result of a three-dimensional simulation under the flow condition corresponding to the experimental result shown in the same color.

and mixing efficiency (Figure 4b) as a function of Q_d/Q_{tot}. Mixing uniformity is equated with the standard deviation of the elapsed time $\sigma_t(x)$; mixing efficiency $\bar{C}/C_B$ is defined as the ratio of the average concentration in the jet to the bulk concentration in the side channels of solute B. Figure 4 shows both parameters at $\langle t \rangle = 1$ ms as the sheath ratio is varied, while Q_c and Q_s are fixed at 1 and 10 μL/min, respectively. As the diagonal flow rate Q_d increases and thus the sheath is thicker, mixing becomes more uniform as desired. Whereas the mixing uniformity remains rather constant for Q_d/Q_{tot} larger than ~1%, a thicker sheath hinders diffusive mixing of reactants as indicated by decreased mixing efficiency. Under the conditions specified here, 1−2% of total flow rate into the diagonal channel improves the mixing uniformity considerably without delaying the mixing process. The optimal value of this parameter depends on experimental factors such as flow velocity, channel width, and the diffusion coefficient of reactants.

(b) Jet Flow Speed. The flow speed of the jet establishes a correspondence between position in the device and time. We used FCS to measure the three-dimensional flow speed profile within the device. We assume a uniform flow speed across the ~3 μm^3 focal volume of the detection beam since it is much smaller than the channel dimension. Figure 5a shows representative cross-correlation curves obtained at different flow speeds. Data acquired in the absence of flow (dotted curve) for calibration purposes yield $\tau_{diff} = (9.8 \pm 0.2) \times 10^{-5}$ s and $r_0 = 344 \pm 8$ nm. Figure 5b shows the results of numerous FCS measurements carried out along the center line of the device ($y = 0$). Jet flow speeds in the useful operating range of the device are plotted as a function of x. Increases in the flow speed that result from hydrodynamic focusing are clearly visible in this figure. Furthermore, the measured profiles of the flow speed agree well with predictions of simulations (lines in Figure 5b). Brister et al. report that the accuracy in r_0 is the largest source of the systematic error in flow velocity measurements using FCS,[38] though we find that uncertainty in both r_0 and τ_{flow} contribute roughly equal amounts to the error in the flow speed measurement. The relative error in flow

(38) Brister, P. C.; Kuricheti, K. K.; Buschmann, V.; Weston, K. D. *Lab Chip* **2005**, *5*, 785−791.

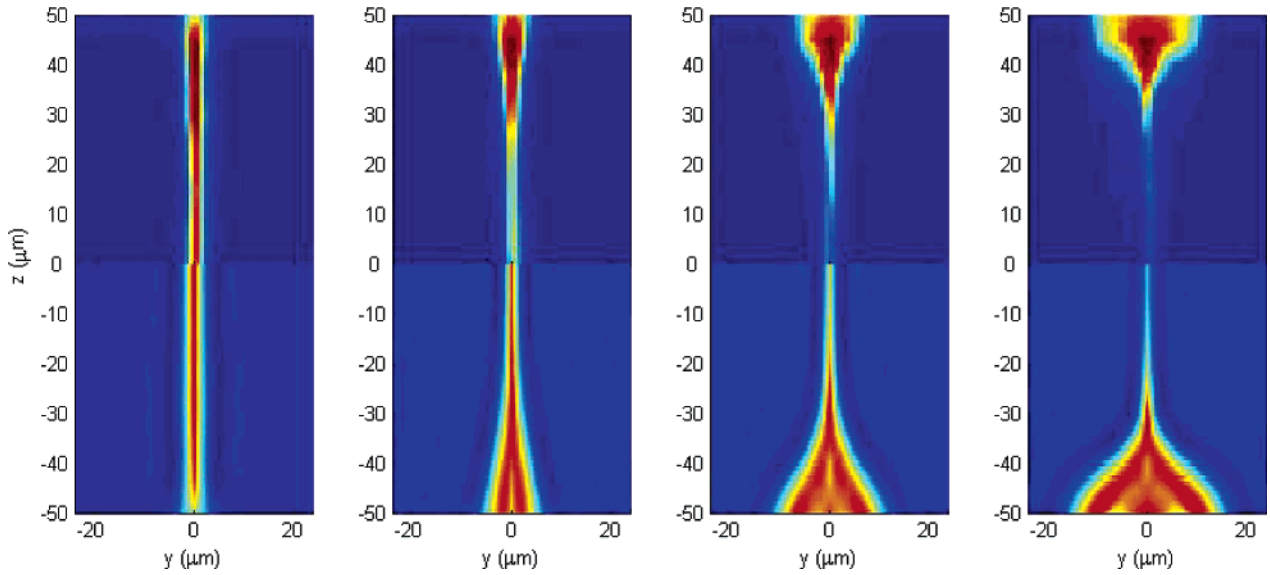

Figure 6. Cross sections of the focused jet at four different flow speeds. The upper halves are multiphoton images of the jet labeled with 50 μM Alexa 488 dextran conjugate 10 kDa. The lower halves are three-dimensional simulation results. The total flow rates are (a) Q_{tot} = 22 μL/min, (b) Q_{tot} =66 μL/min, (c) Q_{tot} = 110 μL/min, and (d) Q_{tot} = 154 μL/min, respectively.

speeds from 1 mm/s to 1 m/s was ~4%. Within the uncertainty of each measurement, the same flow speed was measured in mixers imprinted from the same silicon mold.

Shorter times can be accessed, in theory, by increasing the jet flow speed; however a boundary effect from the channel walls presents a practical upper limit. We measured the vertical jet profile as a function of Q_{tot} while maintaining the ratio between the inlet flow rates (Q_c:Q_d:Q_s = 2:1:20). Cross sections of the hydrodynamically focused jet at x = 200 μm are depicted in Figure 6. The upper half of each panel shows the z-scans of the fluorescently labeled jet measured with multiphoton excitation; the lower half shows the three-dimensional simulation results. In the 50 μm wide and 100 μm deep channel, the z-profile of the jet is uniform at the jet flow speed of ~13 cm/s (see Figure 6a). As the flow speed increases, the three-dimensional pressure gradient present during focusing significantly affects the flow pattern, and the vertical jet profile becomes inhomogeneous (see Figure 5b–d). The jet is broad near the surfaces of the channel, yet thin in the middle. At flow speeds above ~1 m/s, the jet pinches off. Vortices build up at higher flow speeds.[39]

(c) Jet Width. The jet width determines the diffusive mixing time as well as the signal strength. It is controlled experimentally by two factors, the ratio of the center to the total flow rate, Q_c/Q_{tot}, and the absolute value of the total flow rate, Q_{tot}.

To investigate diffusive mixing within the device, we monitored the collisional quenching of fluorescent dye by iodide ions. Using the value of the Stern–Volmer constant k_{SV} = 18.9 ± 0.9 M^{-1} derived from equilibrium measurements, the local concentration of potassium iodide was directly calculated from eq 2. Figure 7 shows the time courses of diffusive mixing into jets with widths ranging from 220 nm to 2.2 μm. The jet width was varied by changing the total flow rate, but fixing the ratio of Q_c to Q_s at 1:10. The sheath flow rate, Q_d, was determined for each flow condition as discussed in the previous section. The location along the outlet channel (x coordinate) was converted into time using the experimentally verified simulation results for the velocity field and eq 5.

If the jet width is known and all artifacts of premixing have been eliminated with sheath flow, the mixing time of the device can be calculated analytically. To test the applicability of the analytic solution, we calculated an effective jet width in the vertical mid-plane of the outlet channel using the positions of the outermost sheath flow streamlines in the three-dimensional simulations. The formulation of the analytical solution is as follows. Suppose macromolecules in solution A are localized in a thin slab in an infinitely wide channel filled with solution B. Solution B will diffuse into the thin slab, and the initial sharp concentration step will broaden gradually until the concentration becomes uniform. From Fick's law of diffusion, the analytical solution for the

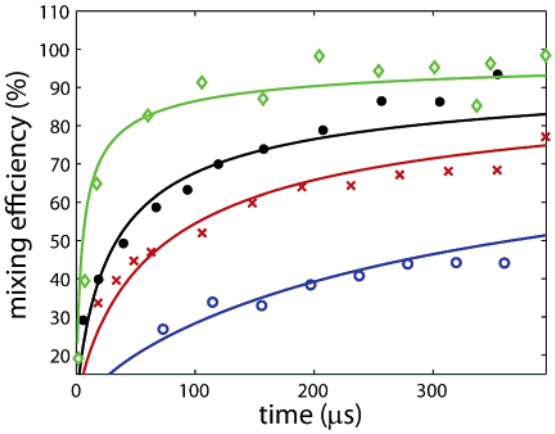

Figure 7. Mixing efficiency as a function of time. The mixing efficiency is shown under the same experimental conditions (and using the same symbols) as Figure 5. The analytical solution for diffusive mixing (eq 8) of iodide ion is shown in solid lines with W = 1.8 μm (blue line), 830 nm (red line), 550 nm (black line), and 220 nm (green line), respectively.

(39) Engler, M.; Kockmann, N.; Kiefer, T.; Woias, P. *Chem. Eng. J.* **2004**, *101*, 315–322.

concentration of solute B is

$$C(t, y) = \frac{C_B}{2}\left\{\text{erfc}\left(\frac{W/2 + y}{\sqrt{4Dt}}\right) + \text{erfc}\left(\frac{W/2 - y}{\sqrt{4Dt}}\right)\right\} \quad (7)$$

where $C(t, y)$ is the concentration of solute B at time t and position y, C_B is the initial concentration of solution B outside of the thin slab, W is the width of the thin slab, and D is the diffusion coefficient of solute B.[40] The average concentration of solute B in the thin slab at time t is calculated by integrating the concentration profile (eq 7) over the width W:

$$\bar{C}(t) = \frac{1}{W}\int_{-\frac{W}{2}}^{\frac{W}{2}} C(t, y)\, dy = C_B\text{erfc}\left(\frac{W}{2\sqrt{Dt}}\right) + \frac{2C_B}{W}\sqrt{\frac{Dt}{\pi}}\{1 - \exp(-W^2/4Dt)\} \quad (8)$$

This formula predicts the mixing efficiency, $\bar{C}/C_B$ in the mixer at time t, given the effective jet width W (slightly less than the jet width plus two sheath widths) and the diffusion coefficient D of the molecule that triggers conformational change.

Figure 7 compares the predictions of the analytical function (eq 8) with the experimental data at various W values: 1.8 μm (blue), 830 nm (red), 550 nm (black), and 220 nm (green), respectively. Just as the theory predicts, mixing accelerates as the jets become thinner. The reasonably good agreement between the experimental data and the analytical solution verifies that the mixing rate depends on the diffusion length and the diffusion coefficient without the complication of premixing. The earliest accessible time $t0$ obtained from the experimentally verified simulation result with threshold concentration of 30% is 35 μs (blue circles), 12 μs (red crosses), 3 μs (black dots), and 2 μs (green diamonds), respectively. With a 220 nm jet, ~80% mixing efficiency is achieved within 60 μs. The mixing time can be enhanced by decreasing the jet width, as long as a sufficient signal is present.

Determination of Time Resolution. Previous hydrodynamic focusing mixers[13,21] display very rapid diffusive mixing times when thin jets are used. For example, Hertzog et al. report 8 μs mixing time using jets as thin as 110 nm.[21] In the experiments of ref 21, the mixing time is defined to be the time it takes for the reactant concentration in the center streamline to increase from 10 to 90% of its value in the side channel. Clearly, the mixing time itself represents an effective error bar and therefore establishes the time resolution of the mixer in the best case scenario (e.g., in the case of very fast flow coupled with very small nozzles, where premixing effect can be neglected). However, if the flow speed is reduced because of inhomogeneous jet profiles (Figure 5) or concerns about sample consumption, or if larger channels are employed due to constraints imposed by the specific detection technique, the uncertainty that arises from premixing along the boundary of the focusing region cannot be ignored. Furthermore, in many macromolecular folding studies, the folding process can be triggered with mixing efficiency significantly below 90%. Under these circumstances, the mixing uniformity becomes the predominant factor in limiting the ultimate time resolution of the device.

A final factor that must be considered in evaluating the time resolution of an experiment is the size of the detection beam. In a typical fluorescence microscope, the focal volume is small, thus the passage time of a molecule through the focal volume may be much shorter than the mixing time. On the other hand, single molecule experiments require very slow flow in order to accumulate sufficient photons for a meaningful measurement, thus the passage time may contribute significantly to the overall time resolution. Furthermore, detection methods such as SAXS or circular dichroism employ relatively large detection beams. The temporal resolution in these measurements is dominated by passage time: the detection beam size divided by the flow speed. Therefore three factors must be considered when determining time resolution: (1) characteristic mixing time, (2) mixing uniformity, and (3) detection time interval.

CONCLUSIONS

We described a novel five-inlet port mixer for investigations of rapid kinetic reactions involving biological macromolecules. Sheath flow from the diagonal channels serves as a barrier between solutions flowing from the center and the two side channels during the focusing process. With minuscule amounts of sheath flow, we demonstrated more than an order of magnitude improvement in mixing uniformity while maintaining rapid diffusive mixing. For applications of this device with fluorescence detection, we fabricated an optically transparent plastic mixer using an imprinting method. Device characterization was carried out using fluorescence correlation spectroscopy (FCS) and two-photon microscopy to measure flow speeds and to quantify diffusive mixing by monitoring the collisional fluorescence quenching, respectively.

In addition to uniform, rapid mixing, other features of this mixer are noteworthy. (1) Unlike turbulent mixers, the entire mixing process is visible. There is no dead time associated with this laminar flow mixer. (2) The sample consumption rate is as low as 10 nL/s due to the moderate jet flow speed of 0.1−1 m/s in this mixer. (3) In contrast to other hydrodynamic focusing mixers, the possibility of protein shearing in the high velocity flow through a small aperture is not an issue. Since this device employs sheath fluid rather than a nozzle, there is much less shear stress involved. (4) Freedom in choosing the channel size is a highly desirable feature because it allows the device to be used with various detection methods using different probe volumes. (5) A practical advantage of the relatively larger channel size is the elimination of clogging; therefore, the mixer can be reliably used for an extended period. (6) The imprinting fabrication method has improved the reproducibility of the mixing process. The device is also inexpensive and disposable because mass production of identical copies is possible. (7) The excellent optical properties of Zeonor, such as high transmittance and low fluorescence background, make these devices well-suited to optical detection techniques. This practical mixer will be a convenient tool for measurements of rapid conformational changes of fluorescently labeled proteins and RNAs.

(40) Cantor, C. R.; Schimmel, P. R. *Biophysical Chemistry*; W. H. Freeman: San Francisco, 1980.

ACKNOWLEDGMENT

The authors thank Sally A. Kim, Jessica S. Lamb, and Kurt Andresen for discussions. This work was supported by the Nanobiotechnology Center (NBTC), an STC Program of the National Science Foundation under Agreement ECS-9876771, and the National Institute of Biomedical Imaging and Bioengineering/ National Institutes of Health Grant 9 P41 EB001976. This work was also supported by Grant P01-GM066275 from the National Institute of General Medical Sciences. All fabrication work was done at the Cornell NanoScale Science & Technology Facility that is supported by the NSF, Cornell University, and industrial affiliates.

Received for review March 29, 2006. Accepted April 17, 2006.

AC060572N